Short solvent model for ion correlations and hydrophobic association

Ang Gao[a,b,c,d], Richard C. Remsing[e], and John D. Weeks[a,b,c,1]

[a]Department of Chemistry and Biochemistry, University of Maryland, College Park, MD 20742; [b]Institute for Physical Science and Technology, University of Maryland, College Park, MD 20742; [c]Chemical Physics Program, University of Maryland, College Park, MD 20742; [d]Institute for Medical Engineering and Science, Massachusetts Institute of Technology, Cambridge, MA 02139; and [e]Department of Chemistry and Chemical Biology, Rutgers University, Piscataway, NJ 08854

Contributed by John D. Weeks, December 3, 2019 (sent for review October 30, 2019; reviewed by Bo Li and Benjamin Widom)

Coulomb interactions play a major role in determining the thermodynamics, structure, and dynamics of condensed-phase systems, but often present significant challenges. Computer simulations usually use periodic boundary conditions to minimize corrections from finite cell boundaries but the long range of the Coulomb interactions generates significant contributions from distant periodic images of the simulation cell, usually calculated by Ewald sum techniques. This can add significant overhead to computer simulations and hampers the development of intuitive local pictures and simple analytic theory. In this paper, we present a general framework based on local molecular field theory to accurately determine the contributions from long-ranged Coulomb interactions to the potential of mean force between ionic or apolar hydrophobic solutes in dilute aqueous solutions described by standard classical point charge water models. The simplest approximation leads to a short solvent (SS) model, with truncated solvent–solvent and solute–solvent Coulomb interactions and long-ranged but screened Coulomb interactions only between charged solutes. The SS model accurately describes the interplay between strong short-ranged solute core interactions, local hydrogen-bond configurations, and long-ranged dielectric screening of distant charges, competing effects that are difficult to capture in standard implicit solvent models.

Coulomb interactions | hydrophobic hydration and association | implicit solvent model | ion correlations

Capturing the flexible multiscale nature of water interactions in solvation and self-assembly processes presents many conceptual and computational challenges. Hydrophobic interactions, where apolar residues cluster together to minimize their contacts with water, are a major driving force in protein folding and the association of lipid molecules to form membranes, vesicles, and micelles (1). Water can also form strong short-ranged directional hydrogen bonds with polar molecules or residues and build hydrogen-bond bridges between them. In addition to this short-ranged physics involving the interplay between molecular cores and solute charges on local hydrogen-bond configurations, water dipoles screen Coulomb interactions between distant charges, with important effects on the initial stages of protein folding, biomolecular assembly, and dielectric properties in general.

Explicitly including water molecules in computer simulations is the most reliable way to describe their variable effects on the behavior of solutions. However, when modeling large and complex solutes or biomolecules, this explicit solvent model becomes computationally expensive, because of the large number of water molecules required to solvate the large molecules and to minimize interactions between periodic images. This is compounded by the need to use special techniques like Ewald summation (2–4) to accurately account for effects of long-ranged Coulomb interactions in periodic simulation cells.

Coarse-grained implicit solvent models (5), where the solvent degrees of freedom are formally integrated out, greatly reduce the number of degrees of freedom and can significantly improve computational efficiency for equilibrium properties. However, an exact coarse-graining procedure generates effective many-body- and state-dependent interactions between the solutes whose consequences are hard to determine in advance and dynamical processes present further difficulties (5).

Many different models have been used to approximate these effective interactions in simpler ways. Most implicit solvent models try to define a fixed boundary around the solutes such that long-ranged interactions outside are screened by a dielectric continuum and short-ranged interactions inside are approximated by effective few-body interactions with simple predetermined functional forms (5–13). Well-known examples include the generalized Born model for dielectric effects (6–9) and the "solvent-accessible surface area model" for nonpolar effects (5, 7, 10, 11). Such models have been shown to qualitatively capture the behavior of the explicit solvent model in many cases (14–19), but often fail when solute charges or configurational changes strongly perturb the local solvent structure (15, 20–25). For example, it is found that these models typically fail to predict the length-scale dependence of hydrophobic interactions (21) or predict the solvent-separated minimum of the potential of mean force (PMF) between charged amino acid side chains (22).

Recent work has shown that the accuracy of implicit solvent models can be improved by using a more realistic solute–solvent

Significance

Solvent-mediated interactions are a major driving force in phenomena ranging from protein folding and ligand–receptor binding to self-assembly. Coulomb interactions in polar solvents like water can act over long ranges, impeding the development of simple local pictures and adding overhead to computer simulations. Here we use local molecular field theory to accurately determine the contributions from long-ranged Coulomb interactions to the potential of mean force between ionic and apolar solutes in dilute aqueous solutions, using results from a "short solvent" system with truncated solvent Coulomb interactions. We anticipate that our approach will facilitate more efficient simulations of large and complex biomolecular and materials systems, in addition to creating a better understanding of solvent effects driven by long-ranged interactions.

Author contributions: A.G. and J.D.W. designed research; A.G., R.C.R., and J.D.W. performed research; A.G., R.C.R., and J.D.W. analyzed data; and A.G., R.C.R., and J.D.W. wrote the paper.

Reviewers: B.L., University of California San Diego; and B.W., Cornell University.

The authors declare no competing interest.

Data deposition: The computer code and data used to generate the results reported here have been deposited on GitHub and can be accessed at https://github.com/andy90/ShortSolventModel.

[1]To whom correspondence may be addressed. Email: jdw@umd.edu.

First published January 7, 2020.

boundary (26–28). For example, the variational implicit solvent model (VISM) determines the position of a flexible solute–solvent boundary by minimizing an approximate VISM solvation free energy functional. It has been shown that the VISM can describe the metastable hydration states and the dry–wet transition that occur during hydrophobic association (27). However, the computational burden for implementing the VISM is nontrivial, and there may be other competing short-ranged effects of solute–solvent interactions not included in the assumed free energy functional. For example, the standard VISM lacks the atomic-scale detail needed to capture subtleties of ionic solvation, such as the asymmetry of the solvation free energy with respect to ion charge for cations and anions of the same size (29).

In this paper, we generalize ideas used in a recent local molecular field (LMF) treatment of solvent structure induced by a fixed solute or by confining walls (30) and the associated free energy changes to develop a theory for the PMF between mobile charged or hydrophobic molecular species in dilute aqueous solutions. The theory here focuses on a particularly simple short solvent (SS) model Hamiltonian where all solvent–solvent and solvent–solute Coulomb interactions are truncated and effective screened solute–solute Coulomb interactions are introduced only between charged solutes. The SS model can be easily incorporated into standard simulation packages and greatly reduces the computational overhead and possible artifacts from standard lattice-sum treatments of long-ranged Coulomb interactions in explicit solvent models while still permitting an accurate molecular-scale description of the complicated short-ranged physics that is difficult to capture in implicit solvent models.

In particular, the computational cost of the traditional Ewald algorithm naively scales with the number of charged sites as N^2, and its most efficient implementations scale as $N \log N$. While the SS model does not alter these basic scaling forms, it drastically reduces the number of sites that have long-ranged Coulomb interactions, such that $N \to N_S \ll N$, where N_S is the number of solute sites. Moreover, the solvent–solvent and solvent–solute interactions, which dominate the computational cost of traditional biomolecular simulations, are purely short ranged in the SS model and therefore scale linearly with the number of solvent sites.

Our starting point is an exact statistical mechanics framework based on the Yvon–Born–Green hierarchy (31) relating correlation functions to intermolecular forces. LMF theory then systematically exploits the slowly varying nature of the long-ranged tails in Coulomb [and sometimes Lennard-Jones (LJ)–type (32)] intermolecular interactions in the Hamiltonian of the full system of interest to define a simpler full mimic (FM) system with Gaussian-truncated (GT) solvent–solvent Coulomb interactions as detailed below and appropriately chosen effective or renormalized solute–solute and solute–solvent interactions. The renormalized interactions analytically incorporate the averaged effects of the long-ranged tails and can be chosen by a self-consistent solution of a simple mean-field–like LMF equation to accurately reproduce relevant solute–solute and solute–solvent correlation functions in the full system.

This allows us to use simulations and theory in the simpler mimic system to determine many desired structural and thermodynamic properties in the full system. The SS system takes this truncation a step farther by using the GT representation of all Coulomb interactions involving the solvent, such that all solvent–solvent and solvent–solute Coulomb interactions are truncated, with renormalized Coulomb tails only between charged solutes.

The solvent in the SS system falls into a broad class of truncated or short water models, which accurately describe local H-bonding and packing interactions but lack the proper long-ranged electrostatics. Other short water models have been generated by reaction-field and other truncated electrostatic methods (33–35), as well as by many machine-learning–based models of water, which typically lack long-ranged interactions beyond the length scale used to train the model (36–38). However, by using simple mean-field–like LMF equations, one can systematically incorporate longer-ranged correlations responsible for dielectric phenomena into these short water models.

We anticipate that the SS model can serve as a useful general alternative to explicit and implicit solvent models in describing the association and configurations of complex molecular solutes and biopolymers in solution, especially in difficult cases where competing short-ranged interactions and water's flexibility obscure a simple physical picture.

For example, it is known that the screened long-ranged Coulomb interactions between biomolecules can dramatically influence their binding rate (39), and with effective solute–solute Coulomb interactions incorporated into the SS model, we expect this behavior can be correctly captured. More generally, we believe LMF theory presents a consistent theoretical framework that can be further developed to yield simplified models permitting more efficient biomolecular simulations while retaining a high level of accuracy and molecular detail.

Theory

Thermodynamic cycles are used to relate properties in mimic systems to those in the full or target system in an LMF approach. Here we first determine the PMF $\omega^{\mathrm{f}}_{\mathrm{AB}}(r)$ for two spherically symmetric charged ions of species A and B in a dilute solution in full solvent W. As schematically illustrated by the orange arrow in Fig. 1, *Top*, this is given by the reversible work or free energy change to move the infinitely separated solutes to a relative separation r or, equivalently, by the free energy difference of

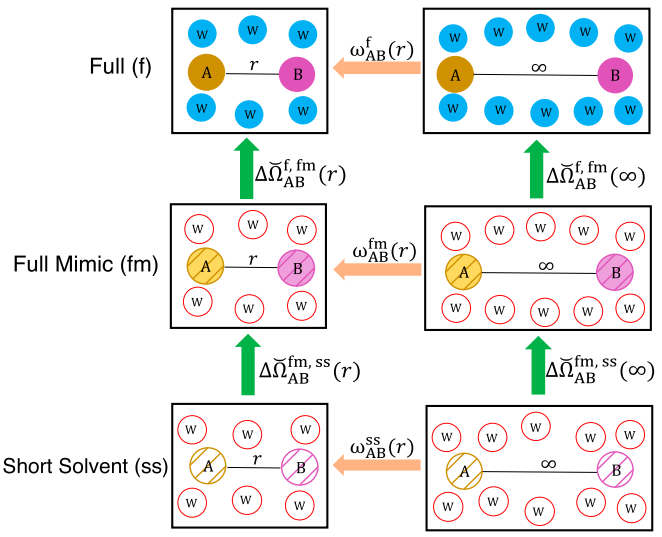

Fig. 1. Thermodynamic cycles that relate the solute–solute PMFs to the solvation free energy differences between the full system, the full mimic system, and the short solvent system. In this example, two ions of species A and B are dilutely solvated in water, denoted as W. In the full system all of the electrostatic interactions are fully taken into account. In the full mimic system the solvent–solvent electrostatic interaction is Gaussian truncated, and effective solute–solvent and solute–solute interactions are introduced. In the short solvent system both the solvent–solvent and solute–solvent electrostatic interactions are Gaussian truncated, and effective interactions are introduced only between solutes. $\Delta\breve{\Omega}^{\mathrm{f,fm}}_{\mathrm{AB}}(r)$ and $\Delta\breve{\Omega}^{\mathrm{fm,ss}}_{\mathrm{AB}}(r)$, represented by green arrows, denote the grand solvation free energy difference between systems with the same solute positions. $\omega^{\mathrm{f}}_{\mathrm{AB}}(r)$, $\omega^{\mathrm{fm}}_{\mathrm{AB}}(r)$, and $\omega^{\mathrm{ss}}_{\mathrm{AB}}(r)$, represented by orange arrows, denote the solute–solute PMF in the full, full mimic, and short solvent systems, respectively.

solvating the two solutes at separation r with respect to solvating them at infinite separation:

$$\omega^{\mathrm{f}}_{\mathrm{AB}}(r) = \Omega^{\mathrm{f}}_{\mathrm{AB}}(r) - \Omega^{\mathrm{f}}_{\mathrm{AB}}(\infty) = \breve{\Omega}^{\mathrm{f}}_{\mathrm{AB}}(r) - \breve{\Omega}^{\mathrm{f}}_{\mathrm{AB}}(\infty). \quad [1]$$

The intensive solvation free energy $\breve{\Omega}^{\mathrm{f}}_{\mathrm{AB}}(r)$ of the solute pair with a fixed relative separation r in the full system (Fig. 1, *Top Left*) is defined as

$$\breve{\Omega}^{\mathrm{f}}_{\mathrm{AB}}(r) \equiv \Omega^{\mathrm{f}}_{\mathrm{AB}}(r) - \Omega^{\mathrm{f}}, \quad [2]$$

where $\Omega^{\mathrm{f}}_{\mathrm{AB}}(r)$ is the (extensive) grand free energy of the full system with A and B solutes at a fixed separation r and Ω^{f} is the grand free energy of bulk full water. When the solute separation tends to infinity, as in Fig. 1, *Top Right*, the solvation free energy of the solute pair is simply the sum of the single-solute free energies:

$$\breve{\Omega}^{\mathrm{f}}_{\mathrm{AB}}(\infty) = \breve{\Omega}^{\mathrm{f}}_{\mathrm{A}} + \breve{\Omega}^{\mathrm{f}}_{\mathrm{B}}. \quad [3]$$

We suppose $\omega^{\mathrm{f}}_{\mathrm{AB}}(r)$ is difficult to calculate in simulations using full explicit water because of inefficient sampling of solute configurations in the dilute solution and overhead and possible artifacts from conventional treatments of the long-ranged Coulomb interactions. LMF approaches define simpler mimic systems with truncated solvent–solvent Coulomb interactions and properly renormalized solute interactions that can accurately approximate this PMF, as schematically depicted in Fig. 1, *Middle* and *Bottom*. The truncation arises from representing the basic Coulomb interaction $v(r) \equiv 1/r$ between solvent charges as a sum of short- and long-ranged components controlled by a smoothing or truncation length σ,

$$v(r) = \frac{\mathrm{erfc}(r/\sigma)}{r} + \frac{\mathrm{erf}(r/\sigma)}{r} = v_0(r) + v_1(r), \quad [4]$$

and ignoring the long-ranged component $v_1(r)$, as illustrated in Fig. 2*C*.

The smoothing length σ is a consistency parameter chosen using physical principles rather than a fitting parameter as used in typical methods for treating long-ranged interactions. In particular, the approximations leading to the LMF equation from the exact YBG hierarchy can be justified for any σ on the scale of characteristic nearest-neighbor charge–charge correlations in the system or larger (30, 31). For water, this corresponds to a minimal value of $\sigma \approx 0.3$ nm, as shown in previous work, and here we make a conservative choice of $\sigma = 0.5$ nm throughout.

The analogous PMF in the simple SS model is depicted in Fig. 1, *Bottom*. Renormalized solutes are introduced with an effective solute–solute pair interaction $\mathrm{w}^{\mathrm{ss}}_{\mathrm{AB}}(r)$ that is to be chosen in principle so that the solute–solute PMFs in the full and SS systems given by the orange arrows are equal: $\omega^{\mathrm{ss}}_{\mathrm{AB}}(r) = \omega^{\mathrm{f}}_{\mathrm{AB}}(r)$. The open circles in Fig. 1, *Bottom* indicate a true "short solvent" where both solvent–solute and solvent–solvent Coulomb interactions are truncated.

When detailed information about solute–solvent pair correlations in the full AB system is also of interest, we can use a more general FM system where only solvent–solvent interactions are truncated, as depicted in Fig. 1, *Middle*. In the FM system both solute–solute and solute–solvent effective interactions are chosen to generate correlation functions that accurately match both the solute–solute and solute–solvent PMFs in the full system. However, self-consistently determining both sets of effective interactions and carrying out simulations in the FM system are computationally more expensive than in the SS system, and the SS model also has more direct connections to implicit solvent models. In this paper we focus mainly on analytic and simulation results for dilute mobile solutes using the SS model, where simple and very accurate results can be consistently derived exploiting only the slowly varying nature of the Coulomb tails.

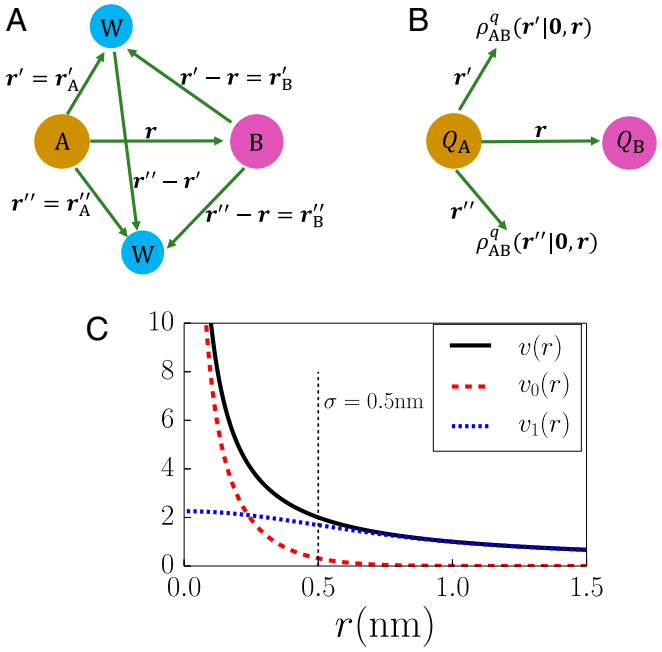

Fig. 2. Notation used in our derivation. (*A*) The coordinates for the solute and solvent particles. Solute A is placed at the origin. Solute B is placed at $\boldsymbol{r}$. Coordinates of solvent W are denoted as $\boldsymbol{r}'$, $\boldsymbol{r}''$, etc. The relative displacement between depicted solvent sites is $\boldsymbol{r}'' - \boldsymbol{r}'$ and their displacements relative to the two solutes are denoted as $\boldsymbol{r}'_{\mathrm{A}}$, $\boldsymbol{r}'_{\mathrm{B}}$, $\boldsymbol{r}''_{\mathrm{A}}$, $\boldsymbol{r}''_{\mathrm{B}}$, etc. (*B*) The associated solvent charge distributions. The charges carried by the two solutes are denoted as Q_{A} and Q_{B}, respectively. The ensemble-averaged water charge density at $\boldsymbol{r}'$ is denoted as $\rho^{q}_{\mathrm{AB}}(\boldsymbol{r}' \mid \boldsymbol{0}, \boldsymbol{r})$. (*C*) Separation of the Coulomb interaction $v(r) = 1/r$ into a short-ranged part $v_0(r) = \mathrm{erfc}(r/\sigma)/r$ and a long-ranged part $v_1(r) = \mathrm{erf}(r/\sigma)/r$. The value of σ controls the truncation or smoothing length, which we choose to be 0.5 nm in this paper, consistent with earlier work.

Vertical green arrows in Fig. 1 give the free energy differences between the various solvent models with the two solutes fixed at the same positions. The upper two green and orange arrows define a thermodynamic cycle that connects the FM system to the full system and a similar cycle in Fig. 1, *Middle* and *Bottom* connects the SS system to the FM system. In particular, the upper left green arrow, denoted as $\Delta\breve{\Omega}^{\mathrm{f,fm}}_{\mathrm{AB}}(r)$, gives the solvation free energy difference between the full and FM systems:

$$\Delta\breve{\Omega}^{\mathrm{f,fm}}_{\mathrm{AB}}(r) \equiv \breve{\Omega}^{\mathrm{f}}_{\mathrm{AB}}(r) - \breve{\Omega}^{\mathrm{fm}}_{\mathrm{AB}}(r). \quad [5]$$

The other green arrows can be similarly defined.

Free energy differences represented by the orange and green arrows in Fig. 1 can be naturally separated into a direct contribution from the pair potential between the fixed AB solutes and the remaining indirect part mediated by the solvent (and other mobile solutes at finite dilution). This separation will prove especially useful in LMF theory, where we want to choose effective pair interactions in the mimic systems to match target correlation functions in the full system.

Thus the upper orange arrow $\omega^{\mathrm{f}}_{\mathrm{AB}}(r)$ in Fig. 1 can be written as

$$\omega^{\mathrm{f}}_{\mathrm{AB}}(r) \equiv \mathrm{w}^{\mathrm{f}}_{\mathrm{AB}}(r) + \bar{\omega}^{\mathrm{f}}_{\mathrm{AB}}(r), \quad [6]$$

where $\mathrm{w}^{\mathrm{f}}_{\mathrm{AB}}(r)$ denotes the known direct AB pair interaction in the full system and $\bar{\omega}^{\mathrm{f}}_{\mathrm{AB}}(r)$ denotes the indirect part of the PMF,

indicated by the overbar symbol. Similarly, the solvation free energy of Fig. 1, *Top Left*, $\breve{\Omega}^{\mathrm{f}}_{\mathrm{AB}}(r)$, can be written as

$$\breve{\Omega}^{\mathrm{f}}_{\mathrm{AB}}(r) \equiv \mathsf{w}^{\mathrm{f}}_{\mathrm{AB}}(r) + \bar{\Omega}^{\mathrm{f}}_{\mathrm{AB}}(r), \qquad [7]$$

where $\bar{\Omega}^{\mathrm{f}}_{\mathrm{AB}}(r)$ denotes the indirect contribution to the solvation free energy.

Free energy differences as in Eq. **5** represented by green arrows in Fig. 1 similarly separate. Thus the upper left green arrow gives

$$\Delta\breve{\Omega}^{\mathrm{f,fm}}_{\mathrm{AB}}(r) \equiv \mathsf{w}^{\mathrm{f}}_{\mathrm{AB}}(r) - \mathsf{w}^{\mathrm{fm}}_{\mathrm{AB}}(r) + \Delta\bar{\Omega}^{\mathrm{f,fm}}_{\mathrm{AB}}(r), \qquad [8]$$

where

$$\Delta\bar{\Omega}^{\mathrm{f,fm}}_{\mathrm{AB}}(r) \equiv \bar{\Omega}^{\mathrm{f}}_{\mathrm{AB}}(r) - \bar{\Omega}^{\mathrm{fm}}_{\mathrm{AB}}(r). \qquad [9]$$

As in Eq. **3**, when $r \to \infty$, we have

$$\Delta\breve{\Omega}^{\mathrm{f,fm}}_{\mathrm{AB}}(\infty) = \Delta\bar{\Omega}^{\mathrm{f,fm}}_{\mathrm{AB}}(\infty) = \Delta\bar{\Omega}^{\mathrm{f,fm}}_{\mathrm{A}} + \Delta\bar{\Omega}^{\mathrm{f,fm}}_{\mathrm{B}}, \qquad [10]$$

where $\Delta\bar{\Omega}^{\mathrm{f,fm}}_{\mathrm{A}}$ is the difference between the solvation free energies for a single A solute in the full and full mimic systems.

We can easily derive equations for the desired effective potentials in each cycle in terms of these quantities. Effective solute–solvent and solute–solute interactions in the FM system and only solute–solute interactions in the simpler SS system are supposed to be chosen such that all orange arrows in Fig. 1 are equal:

$$\omega^{\mathrm{f}}_{\mathrm{AB}}(r) = \omega^{\mathrm{fm}}_{\mathrm{AB}}(r) = \omega^{\mathrm{ss}}_{\mathrm{AB}}(r). \qquad [11]$$

Because the net free energy change around any cycle is zero, this equivalence implies that the right and left green arrows in Fig. 1 in each cycle are equal and independent of r:

$$\Delta\breve{\Omega}^{\mathrm{f,fm}}_{\mathrm{AB}}(r) = \Delta\breve{\Omega}^{\mathrm{f,fm}}_{\mathrm{AB}}(\infty) = \Delta\bar{\Omega}^{\mathrm{f,fm}}_{\mathrm{A}} + \Delta\bar{\Omega}^{\mathrm{f,fm}}_{\mathrm{B}}, \qquad [12]$$

$$\Delta\breve{\Omega}^{\mathrm{fm,ss}}_{\mathrm{AB}}(r) = \Delta\breve{\Omega}^{\mathrm{fm,ss}}_{\mathrm{AB}}(\infty) = \Delta\bar{\Omega}^{\mathrm{fm,ss}}_{\mathrm{A}} + \Delta\bar{\Omega}^{\mathrm{fm,ss}}_{\mathrm{B}}. \qquad [13]$$

Eq. **12** combined with Eqs. **8** and **10** gives us an exact expression for the required AB interaction in the FM system:

$$\mathsf{w}^{\mathrm{fm}}_{\mathrm{AB}}(r) = \mathsf{w}^{\mathrm{f}}_{\mathrm{AB}}(r) + \Delta\bar{\Omega}^{\mathrm{f,fm}}_{\mathrm{AB}}(r) - \Delta\bar{\Omega}^{\mathrm{f,fm}}_{\mathrm{A}} - \Delta\bar{\Omega}^{\mathrm{f,fm}}_{\mathrm{B}}. \qquad [14]$$

A similar exact result for the SS model can be found by matching the green arrows in the lower cycle in Fig. 1:

$$\mathsf{w}^{\mathrm{ss}}_{\mathrm{AB}}(r) = \mathsf{w}^{\mathrm{fm}}_{\mathrm{AB}}(r) + \Delta\bar{\Omega}^{\mathrm{fm,ss}}_{\mathrm{AB}}(r) - \Delta\bar{\Omega}^{\mathrm{fm,ss}}_{\mathrm{A}} - \Delta\bar{\Omega}^{\mathrm{fm,ss}}_{\mathrm{B}}. \qquad [15]$$

Combining Eqs. **14** and **15**, this can be rewritten as

$$\begin{aligned}\mathsf{w}^{\mathrm{ss}}_{\mathrm{AB}}(r) = \mathsf{w}^{\mathrm{f}}_{\mathrm{AB}}(r) &+ \Delta\bar{\Omega}^{\mathrm{f,fm}}_{\mathrm{AB}}(r) - \Delta\bar{\Omega}^{\mathrm{f,fm}}_{\mathrm{A}} - \Delta\bar{\Omega}^{\mathrm{f,fm}}_{\mathrm{B}} \\ &+ \Delta\bar{\Omega}^{\mathrm{fm,ss}}_{\mathrm{AB}}(r) - \Delta\bar{\Omega}^{\mathrm{fm,ss}}_{\mathrm{A}} - \Delta\bar{\Omega}^{\mathrm{fm,ss}}_{\mathrm{B}}.\end{aligned} \qquad [16]$$

Eqs. **14** and **16** exactly relate the desired effective potentials in each cycle to the free energy differences on the right-hand sides as given by the indirect parts of the green arrows in Fig. 1. These can be accurately approximated by building on previous LMF results by Remsing et al. (30), which considered directly analogous processes involving a single fixed solute. As shown in *Materials and Methods*, which discusses the additional complications that arise in the present case with two mobile solutes, the resulting equations provide simple and generally accurate LMF-based approximations for the indirect contributions like $\Delta\bar{\Omega}^{\mathrm{f,fm}}_{\mathrm{AB}}(r)$ and $\Delta\bar{\Omega}^{\mathrm{fm,ss}}_{\mathrm{AB}}(r)$ appearing in Eqs. **14** and **16**.

With the approximations detailed in *Material and Methods* made, Eq. **16** reduces to the following simple expression for the effective solute–solute potential $\mathsf{w}^{\mathrm{ss}}_{\mathrm{AB}}(r)$ in the short solvent system:

$$\begin{aligned}\mathsf{w}^{\mathrm{ss}}_{\mathrm{AB}}(r) &= \mathsf{w}^{\mathrm{f}}_{\mathrm{AB}}(r) \\ &+ \frac{1}{2}\int d\boldsymbol{r}'\left(\rho^{q}_{\mathrm{A}}(\boldsymbol{r}'_{\mathrm{A}}) + \rho^{q}_{0,\mathrm{A}}(\boldsymbol{r}'_{\mathrm{A}})\right) Q_{\mathrm{B}}\, v_1(r'_{\mathrm{B}}) \\ &+ \frac{1}{2}\int d\boldsymbol{r}'\left(\rho^{q}_{\mathrm{B}}(\boldsymbol{r}'_{\mathrm{B}}) + \rho^{q}_{0,\mathrm{B}}(\boldsymbol{r}'_{\mathrm{B}})\right) Q_{\mathrm{A}}\, v_1(r'_{\mathrm{A}}) \\ &+ \frac{1}{2}\iint d\boldsymbol{r}'\, d\boldsymbol{r}''\left(\rho^{q}_{\mathrm{A}}(\boldsymbol{r}'_{\mathrm{A}})\rho^{q}_{0,\mathrm{B}}(\boldsymbol{r}''_{\mathrm{B}})\right. \\ &\left. + \rho^{q}_{\mathrm{B}}(\boldsymbol{r}'_{\mathrm{B}})\rho^{q}_{0,\mathrm{A}}(\boldsymbol{r}''_{\mathrm{A}})\right) v_1(|\boldsymbol{r}'' - \boldsymbol{r}'|).\end{aligned} \qquad [17]$$

For the simple ion models used here the direct ion–ion interaction $\mathsf{w}^{\mathrm{f}}_{\mathrm{AB}}(r) \equiv \mathsf{w}^{\mathrm{f}}_{\mathrm{ne,AB}}(r) + Q_{\mathrm{A}}\, Q_{\mathrm{B}}\, v(r)$ has a nonelectrostatic component $\mathsf{w}^{\mathrm{f}}_{\mathrm{ne,AB}}(r)$ given by the LJ ion–ion pair potential and the electrostatic potential $Q_{\mathrm{A}}\, Q_{\mathrm{B}}\, v(r)$ between the embedded ion charges.

Determining the renormalized interaction in the SS model using Eq. **17** requires only singlet solvent charge densities like ρ^{q}_{A} and $\rho^{q}_{0,\mathrm{A}}$ induced by the hydration of isolated solutes in the full and SS systems (denoted by the subscript 0), respectively. With this in hand, we can use results from simulations or theory in the simple SS model to provide accurate LMF-based approximations for the solute–solute potential of mean force driving ionic association in the full system.

Eq. **17** can also be applied to uncharged (hydrophobic) solutes by setting the ion charges to zero, and the last term, accounting for long-ranged Coulomb interactions between solvent molecules, would in principle still make a contribution to the effective AB pair potential. However, it is generally very small compared to the bare (nonelectrostatic) AB potential $\mathsf{w}^{\mathrm{f}}_{\mathrm{ne,AB}}(r)$, as illustrated below. Thus in most cases corrections from truncation of solvent Coulomb interactions on uncharged solutes in the SS model can be neglected and their PMF in the SS model using the unmodified $\mathsf{w}^{\mathrm{f}}_{\mathrm{ne,AB}}(r)$ accurately approximates that in the full system.

Results

Salt Ions in Water. We first test our theory by studying thermodynamic and structural properties of dilute aqueous solutions of NaCl and $CaCl_2$. Salt ions are widely present in chemical and biological environments and are of vital importance to the biochemical activities of cells. It has been shown that the collective movement of water molecules plays an essential role in the dissociation of ion pairs. Geissler et al. (40) and Ballard and Dellago (41) showed that the dissociation of the $Na^{+}Cl^{-}$ pair is driven by the addition of water molecules into the first solvation shell of the ions. Salanne et al. (42) showed that similar events happen during the dissociation of $Ca^{+2}Cl^{-}$. The usual implicit solvent model cannot capture the motion of solvent molecules and as a result gives a poor ion–ion PMF, as shown by Ballard and Dellago (41).

We obtain the cation–anion PMF by performing biased MD simulation using umbrella sampling and the weighted histogram analysis method (WHAM) (43–46). The force-field parameters used for the ions and water are detailed in *Materials and Methods*. We note that a complete understanding of the hydration structure of monatomic ions is still an active area of investigation, including subtleties associated with charge transfer, polarization effects, and many-body interactions that can be important even for Na^{+} and Cl^{-} (47–51). The outcomes of this ongoing research will be especially important with regard to the refinement of empirical force fields. The choice of

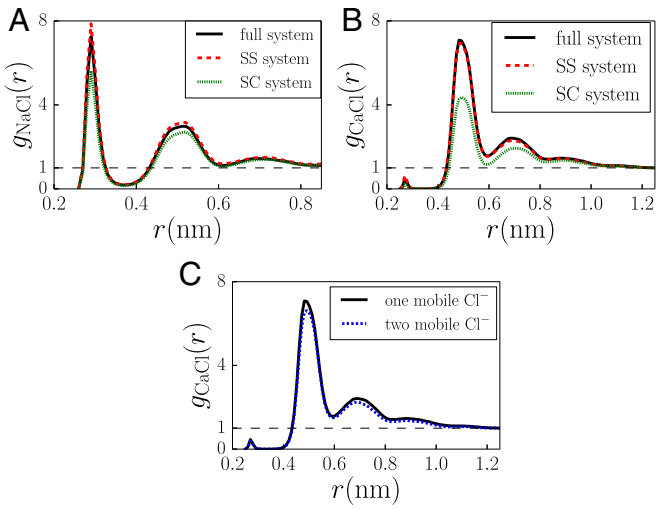

Fig. 3. The ion–ion RDF. (*A*) The $Na^{+}Cl^{-}$ RDF in the full system, the SS system, and the SC system. (*B*) The $Ca^{+2}Cl^{-}$ RDF in the full system, the SS system, and the SC system. (*C*) The $Ca^{+2}Cl^{-}$ RDF in a full system with only one mobile Cl^{-} ion in the simulation box with a uniform neutralizing background (black) and with two mobile Cl^{-} ions in the simulation box.

models for Ca^{+2} is a particularly active area of investigation (52). Recently, it has been suggested that the divalent charge of Ca^{+2} might produce significant polarization effects (53) and further insights from ab initio simulations might be necessary (54).

Here we use highly studied models of Na^{+} and Cl^{-}, as well as a recent classical Ca^{+2} point charge model, which was specifically designed to reproduce equilibrium ion solvation and pairing properties (55). Our goal here is to assess the quantitative accuracy of the LMF-based SS model for a given reasonable choice of model potentials rather than trying to find the "best" ion force fields. Our method of determining the renormalized potentials in the SS model should be applicable to other choices of core potentials as well, since we average only over uniformly slowly varying long-ranged components in its derivation.

Fig. 3 compares the cation–anion radial distribution function (RDF) in full water to that in the SS model, which has GT ion–water and water–water electrostatic interactions with full LJ interactions everywhere. The renormalized ion–ion electrostatic interaction is determined by Eq. **17**, which is shown in *Materials and Methods* to yield a renormalized Coulomb interaction screened by the full bulk dielectric constant ϵ going asymptotically as $Q_A Q_B/\epsilon r$. Since this is still long ranged, effects from periodic images in the SS simulation are taken into account using Ewald sums, but this is needed only between the dilute ion charges.

Fig. 3*C* shows that very similar results are found for the cation–anion RDF for $CaCl_2$ in full water using a neutral simulation box with one cation and two mobile anions or a box with only one mobile anion and a uniform neutralizing background. This indicates that comparison of single cation–anion PMFs in dilute $Na^{+}Cl^{-}$ and $Ca^{+2}Cl^{-}$ and related models is justified because the single-ion PMFs are not significantly altered by neutralization through another mobile ion or by a uniform background charge density.

Also shown in Fig. 3 are results from a strictly short-ranged "strong coupling" or "short Coulomb" (SC) model system where all Coulomb interactions, including those between the ions, are Gaussian truncated. The SC system accurately describes the short-ranged physics involving packing and strong local Coulomb interactions between neighboring ion cores and the local hydrogen-bond configurations around them, but it is not able to capture any effects of dielectric screening on the ion–ion PMF.

As shown in Fig. 3, the full and SS systems give almost identical ion–ion RDFs for both NaCl and $CaCl_2$ while the SC system gives a significantly lower main ion–ion peak. Moreover, there is a dramatic difference in the heights of the first contact ion-pair (CIP) peak and the second solvent-separated ion-pair (SSIP) peak between NaCl and $CaCl_2$. There also exists experimental evidence (56) supporting these differences.

Much of the dominant physics is short ranged and thus is qualitatively captured even by the SC model, but it completely ignores the longer-ranged electrostatic interactions between the ions and water in the full system. The renormalized ion–ion interactions in the SS model account for the subtle but quantitatively important corrections from long-ranged Coulomb interactions and the very good agreement with the full system provides strong support for the accuracy of the general mapping framework depicted in Fig. 1. The differences between the SS and SC systems highlight the importance of dielectric response in determining ion–ion correlations, even at the small length scales typical of SSIPs.

This striking difference between the $Ca^{+2}Cl^{-}$ and $Na^{+}Cl^{-}$ RDFs must result from the higher charge of the Ca^{+2} ion, since both cations have very similar LJ parameters. To verify this point we simulated the association of Na^{+Q} and Cl^{-} in water, where Na^{+Q} is an artificial ion that has the same LJ core as Na^{+} but carries a charge $+Q$. We gradually increased Q from 1 to 2 in a system with a uniform neutralizing background charge. As shown in Fig. 4*A*, the CIP peak initially increases, as would be expected physically from the stronger short-ranged cation–anion attraction, and reaches a maximum at $Q \approx 1.5$. The CIP peak then drops rapidly with increasing Q. At $Q = 2$, the CIP peak is much lower than the SSIP peak, just as is found for $Ca^{+2}Cl^{-}$ association.

This behavior arises from a competition between the increasing contact cation–anion attraction and the collective changes of the water structure and hydrogen-bond configurations around the ions driven by the charging process. To get a better understanding of the mechanism, we monitored the number of water molecules in the first solvation shell of Na^{+Q} when Na^{+Q} and Cl^{-} cores are in contact. As shown in Fig. 4*B*, the number of water molecules around Na^{+Q} remains essentially constant until $Q \approx 1.8$, after which it rapidly increases. This phase-transition–like behavior strongly suggests that the drop of the CIP peak height is driven by the addition of another water molecule into

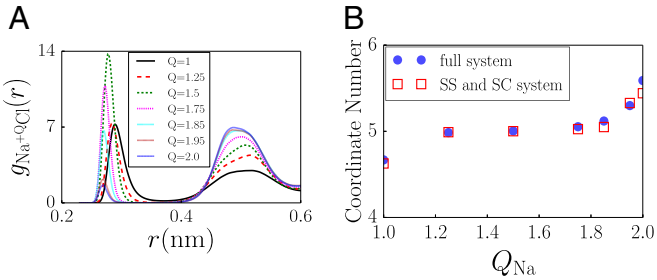

Fig. 4. The ion–ion RDF with variable cation charge Q and the coordination number of water in the first solvation shell. (*A*) The $Na^{+Q}Cl^{-}$ RDF with Q ranging from 1 to 2. (*B*) The number of water molecules in the first solvation shell of Na^{+Q} when Q is increased from 1 to 2. The Na^{+Q} and Cl^{-} ions are kept in contact during the charging process. Blue circles denote the results of the full system. Red squares denote the results of the SS and SC systems. (The SS and SC systems give the same result since they have the same ion–water interaction.)

the first solvation shell of the cation, consistent with previous work examining the role of hydration shell fluctuations in ionic assembly (42, 54, 57).

The complicated interplay between strong short-ranged Coulomb and LJ core forces generating hydrogen bonds and local contributions to ion–water and ion–ion association and the long-ranged Coulomb interactions that determine dielectric screening between distant charges is again quantitatively captured in the SS model. A proper description of this balance, and therefore ionic correlations, is crucial for even qualitative modeling of more complex materials and biophysical systems.

Indeed, divalent metal ions are found to specifically adsorb to fatty acid interfaces relevant to atmospheric chemistry (58), and ionic charge densities ultimately dictate fundamental reactions that underlie complex kinetic processes in an array of settings (59, 60). Moreover, it has been found that the interactions of divalent ions with biomolecules can significantly impact conformational preferences of the latter in a manner that depends sensitively on ion–biomolecule interactions (61–64). We expect that the SS model can be extended to model such complex systems without the need for explicit representation of long-ranged electrostatics.

Nonpolar and Hydrophobic Solutes in Water. We next examine aqueous association of nonpolar solutes of varying sizes, which can generate a length-scale–dependent transition in the nature of the local solute–water interface (65–67). Small solutes are modeled by argon, whose core diameter is about 0.34 nm, small enough that the local hydrogen-bond network around it remains essentially intact (although with reduced fluctuations relative to bulk). A physically suggestive discussion of some of the relevant physics in this regime is given in ref. 68.

Large apolar solutes are modeled as C_{60} fullerenes, each described using the single-site coarse-grained model of Girifalco (69, 70), which has a core diameter of ∼1 nm. The specific force fields used are detailed in *Materials and Methods*.

The PMF between the two fullerene solutes is computed by performing biased simulations using umbrella sampling in conjunction with WHAM (43–46). The fullerene cage is large enough to significantly disrupt and break the hydrogen-bond network near its surface, creating a soft interface with large density fluctuations. However, fullerene–water LJ attractions are strong enough that the average water density near the cage is significantly higher than in the bulk; i.e., the surface is wet by water.

For the small Ar solutes, the PMF shown in Fig. 5*A* exhibits a global minimum at solute–solute contact and a local minimum corresponding to solvent-separated solutes, with a barrier separating the two minima physically arising from the removal of a water molecule from the region between the solutes. Because the hydrogen-bond network remains intact around such small solutes, this necessarily involves breakage of a hydrogen bond. Since the association of two small solutes is dominated by changes in the local hydrogen-bond network, the PMFs are virtually unaffected by Gaussian truncation of solvent–solvent electrostatic interactions, consistent with previous work (71, 72).

Long-ranged electrostatics also have only a small impact on the association free energies of large fullerene solutes, as shown in the upper part of Fig. 5*B*. However, the very strong van der Waals (VDW) solute–solute attractions play a significant role in this solute size regime, competing with hydrophobic interactions, and the solvent-mediated part of the PMF is weakly repulsive at small separations.

To provide a more stringent test of LMF theory for very strong hydrophobic interactions we also considered the association of repulsive-core Weeks–Chandler–Andersen (WCA)

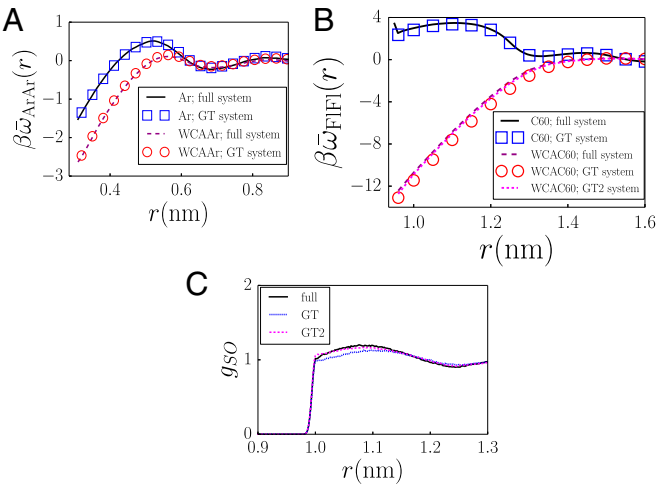

Fig. 5. (*A*) The solvent-mediated part of PMF between argon in full water (black solid line), between argon in GT water (blue square), between WCA argon in full water (purple dashed line), and between WCA argon in GT water (red circle). (*B*) The solvent-mediated part of PMF between fullerenes in full water (black solid line), between fullerenes in GT water (blue square), between WCA fullerenes in full water (purple dashed line), and between WCA fullerenes in GT water (red circle). (*C*) The radial distribution function between the solute and oxygen site of water in full water (black solid line), GT water (blue dashed line), and GT2 water (magenta dashed line). The solute is a harshly repulsive-core solute with 2 nm diameter.

versions of both the Ar and fullerene solutes, where both solute–water and solute–solute VDW attractions are turned off. Understanding the changes in hydrophobic interactions resulting from VDW solute–solvent and solvent–solvent attractions has been the focus of much recent work (72–75). As shown in Fig. 5*A*, the increase in the solvent-mediated hydrophobic attraction between the small purely repulsive Ar solutes is quantitatively captured by the GT or SC system, consistent with minimal corrections from long-ranged electrostatics.

However, when all VDW interactions are truncated for the large fullerenes, the purely repulsive fullerene cores experience an exceptionally strong hydrophobic attraction of order 12 k_BT at contact, as shown in the lower part of Fig. 5*B*. Simulations using unmodified GT water in the SS model qualitatively capture almost all of the dramatic changes that truncation of the VDW interactions induce in the PMF between large full and repulsive-core fullerene solutes. However, small quantitative differences on the order of the thermal energy between the full and GT systems can be seen.

Fig. 5*B* shows that the hydrophobic interaction between repulsive-core fullerenes is slightly stronger in GT water than in full water. Additionally, our earlier work has shown that the solvation free energy of a single large hydrophobic solute is slightly more favorable in GT water than in full water (71). These observations are consistent with easier drying in GT water than in the full water, resulting in increased hydrophobicity of the solutes (71).

A simple empirical way to correct the increased drying for strongly hydrophobic solutes in the GT model while still truncating Coulomb interactions is to slightly reduce the water–water LJ attractions, whose unbalanced effects are known to be the dominant force leading to drying (71, 76, 77). This modified solvent model is designated as the GT2 model. It contains the same Gaussian-truncated Coulomb interactions as in the GT model and modified solvent LJ

interactions $u_\xi(r)$ whose attractive forces are scaled by a coupling parameter ξ:

$$u_\xi(r) = u_0(r) + \xi u_1(r). \quad [18]$$

The potential $u_\xi(r)$ is continuous for all values of ξ, with $\xi = 1$ giving the full oxygen LJ potential in the GT model and $\xi = 0$ the repulsive-core LJ potential, giving the Gaussian-truncated repulsive-core (GTRC) water model discussed in refs. 71 and 77.

Bulk hydrogen-bond patterns and fluctuations in both GT and GT–repulsive-core water, controlled by the strong short-ranged core forces, accurately reproduce those of full bulk water (71, 77), and these should continue to be accurate for any intermediate ξ value in GT2 water. We determined ξ for the GT2 model by requiring that the (oxygen) density distribution of GT2 water around a large, hard-sphere solute match that in full extended simple point charge model (SPC/E) water. Our goal here is to refine the description of hydrophobicity for large repulsive solutes in GT2 water, rather than to try to improve its predictions for general thermodynamic properties of bulk water. At 300 K and 1 atm, a slight reduction in the strength of water–water LJ attractions to $\xi = 0.95$ gives an excellent approximation to the full water density profile (Fig. 5*C*).

With the slight overdrying around a large hydrophobic solute corrected by the reduced ξ in the GT2 model, the truncated (WCAC60) fullerene–fullerene PMF in the full system is quantitatively recovered in simulations using GT2 water, with no explicit corrections from long-ranged Coulomb tails, as shown in Fig. 5*B*. We also verified that the solvation free energy of a single large hard-sphere solute is quantitatively reproduced in the GT2 model as well. The solvation free energy (kJ/mol) values of a 1-nm diameter hard sphere in SPC/E, GT, and GT2 water at 300 K and 1 atm are 480.3, 457.1, and 479.9, respectively.

The fact that fixing the drying around a single large repulsive solute simultaneously fixes its solvation free energy and the pair PMF can be well understood by LMF theory, given that the GT2 and SPC/E models share the same short-ranged core potentials and differ only in their long-ranged interactions. The essentially identical nonuniform density profiles, according to LMF theory, imply that the net unbalanced force coming from long-ranged interactions should also be the same in these two models. LMF solvation theory (30) and the discussion here in *Materials and Methods* have formulated the long-ranged contribution to the solvation and association free energies in terms of the nonuniform density profiles. With these matched in the GT2 model, we would expect that solvation and association free energies are also well reproduced.

Discussion

LMF theory has been applied successfully in diverse scenarios, many of which are beyond the scope of conventional mean-field treatments. It has been shown that LMF theory can very accurately describe drying near a hydrophobic solute in water, overcharging near a highly charged colloid, dielectric screening of a charged ion, and the induced water structure near hydrophobic or charged walls. A recent extension of LMF theory, the symmetry-preserving mean-field theory, has been proved to be able to capture both the equilibrium and dynamical effects of electrostatics at interfaces with high symmetry (78–81).

Most relevant to the present work is the recent extension of LMF theory to determine contributions from the long-ranged Coulomb interactions to free energies of solvation and alchemical transformations of a single solute in water, where the solute–solvent interaction in the mimic system was represented by an effective external field (30, 82). Very accurate estimates of solvation free energies were obtained from a simple analytic expression that requires only knowledge of the effective field and the induced nonuniform singlet charge density.

In this work, we have further extended LMF theory to construct a short solvent model that yields very accurate association energies for ionic and hydrophobic solutes in dilute aqueous solutions. This SS model utilizes a Gaussian truncation of solvent–solvent electrostatics and renormalizes the solute–solute electrostatic interactions according to an LMF theory-based framework, thus avoiding possible artifacts and computational expense arising from standard treatments of long-ranged solvent interactions in periodic systems. We have demonstrated the exceptional accuracy of this approach in describing the association of ionic and hydrophobic solutes in dilute aqueous solutions.

Moreover, the class of GT water models used in the SS system, as well as other short water models mentioned in the Introduction, can also be systematically corrected within the LMF framework to describe both solute–solvent and solute–solute correlations using the full mimic system as depicted in Fig. 1, *Middle*.

To implement the SS model in the context of biomolecular assembly, the simplest approach would be to apply renormalized interactions between each pair of atoms on the biomolecules. However, complications may arise from bonding and geometrical complexities of biomolecules in different configurations (83). For example, most biomolecules possesses both hydrophobic and hydrophilic regions, and extended hydrophobic regions from conformational changes induce very different local solvent structures and fluctuations than seen near hydrophilic regions. As a consequence one needs to take into account the heterogeneous solvation states of extended regions on the biomolecules when trying to determine the renormalized interactions. LMF theory gives a natural framework to address such issues (84) and we are actively working on its implementation in a generalized SS model that we believe can accurately capture the association thermodynamics of biomolecules.

Materials and Methods

Force Field Used in Simulation. Each ion is modeled as a nonpolarizable single-site LJ particle with a point charge at its center. The LJ parameters for Na^+ and Cl^- are those listed by Koneshan et al. (52). The Ca^{2+} parameters are those of Mamatkulov, Fyta, and Netz (55). The ion–ion and ion–water cross-interaction parameters are determined by Lorentz–Berthelot mixing rules. Table 1 summarizes the parameters used for the ions, Ar, and water. To model fullerene, we adopt the coarse-grained model of Girifalco (69, 70).

Magnitude of the Last Term of Eq. 17 for Apolar Solutes. The last term of Eq. **17** has been calculated for various apolar solutes, and its magnitude is found to be very small: It is smaller than 0.007 k_BT when the solute is argon, it is smaller than 0.01 k_BT when the solute is repulsive-core argon, it is smaller than 0.05 k_BT when the solute is fullerene, and it is smaller than 0.05 k_BT when the solute is repulsive-core fullerene. Results are obtained at 300 K and 1 atm, with solvent being SPC/E water.

Adapting Remsing et al. (30) Results to Current Work. Remsing et al. (30) discussed LMF predictions for the solvation free energy of a single ionic

Table 1. Force-field parameters for ions, water, and argon

Atom type	σ(nm)	ϵ(kJ/mol)	Charge
Na^+	0.2586	0.4184	1
Ca^{+2}	0.241	0.94	2
Cl^-	0.4404	0.4184	−1
OW	0.3166	0.6502	−0.8476
HW	0	0	0.4238
Ar	0.34	0.9977	0

solute A fixed at the origin in solvent W. We can immediately adapt many of their results to the system of interest here by considering the electrostatic potential at $\boldsymbol{r}'$ generated by Coulomb interactions from two solutes of types A and B fixed at positions **0** and $\boldsymbol{r}$ as shown in Fig. 2. In the full system, using standard ion models with point charges Q_A and Q_B embedded at the centers of spherically symmetric cores, this has the simple form

$$\mathcal{V}^{f}_{AB}(\boldsymbol{r}'|\mathbf{0},\boldsymbol{r}) \equiv \mathcal{V}_{AB}(\boldsymbol{r}'|\mathbf{0},\boldsymbol{r}) = Q_A v(\boldsymbol{r}'_A) + Q_B v(\boldsymbol{r}'_B). \quad [19]$$

Using Eq. **4** this has short- and long-ranged components

$$\mathcal{V}_{AB}(\boldsymbol{r}'|\mathbf{0},\boldsymbol{r}) = \mathcal{V}_{0,AB}(\boldsymbol{r}'|\mathbf{0},\boldsymbol{r}) + \mathcal{V}_{1,AB}(\boldsymbol{r}'|\mathbf{0},\boldsymbol{r}). \quad [20]$$

The analogous renormalized potential in the FM system is

$$\mathcal{V}^{fm}_{AB}(\boldsymbol{r}'|\mathbf{0},\boldsymbol{r}) \equiv \mathcal{V}_{R,AB}(\boldsymbol{r}'|\mathbf{0},\boldsymbol{r}) = \mathcal{V}_{0,AB}(\boldsymbol{r}'|\mathbf{0},\boldsymbol{r}) + \mathcal{V}_{R1,AB}(\boldsymbol{r}'|\mathbf{0},\boldsymbol{r}). \quad [21]$$

Here we use the subscript R to denote the renormalized solute–solvent interactions in the FM system, with a long-ranged component $\mathcal{V}_{R1}$ chosen to match the induced solvent charge density in the full system, as was done in Remsing et al. (30) for a single isolated solute. In the simpler SS system, the solute–solvent interaction, by definition, has only the short-ranged component:

$$\mathcal{V}^{ss}_{AB}(\boldsymbol{r}'|\mathbf{0},\boldsymbol{r}) = \mathcal{V}_{0,AB}(\boldsymbol{r}'|\mathbf{0},\boldsymbol{r}). \quad [22]$$

$\mathcal{V}_{R,AB}$ in Eq. **21** is accurately given by a natural generalization of the single-solute Coulomb LMF equation in equation 7 of Remsing et al. (30), which can be written as

$$\mathcal{V}_{R,AB}(\boldsymbol{r}'|\mathbf{0},\boldsymbol{r}) = \mathcal{V}_{AB}(\boldsymbol{r}'|\mathbf{0},\boldsymbol{r}) + \int d\boldsymbol{r}''\, \rho^{q}_{AB}(\boldsymbol{r}''|\mathbf{0},\boldsymbol{r}) v_1(|\boldsymbol{r}' - \boldsymbol{r}''|), \quad [23]$$

where, by construction, we have assumed that the induced charge densities in the full and FM systems are equal, $\rho^{q}_{R,AB} = \rho^{q}_{AB}$, when the self-consistent Eq. **23** is satisfied.

Equation 12 of Remsing et al. (30) shows that LMF theory can give very accurate results for the contribution of long-ranged Coulomb interactions to the solvation free energy of a single ionic solute from a simple analytic formula that requires knowledge only of the renormalized potential and the induced charge density. The LMF prediction for the solvent-mediated (or indirect) component of the solvation free energy change, $\Delta\bar{\Omega}^{f,fm}_{AB}(r)$, for the FM system appearing in Eqs. **14** and **16**, is directly analogous to the single-solute result given in equation 12 of Remsing et al. (30) and is given by

$$\Delta\bar{\Omega}^{f,fm}_{AB}(r) = -\frac{1}{2}\int d\boldsymbol{r}'\, \rho^{q}_{AB}(\boldsymbol{r}'|\mathbf{0},\boldsymbol{r}) \cdot \left(\mathcal{V}_{R,AB}(\boldsymbol{r}'|\mathbf{0},\boldsymbol{r}) - \mathcal{V}_{AB}(\boldsymbol{r}'|\mathbf{0},\boldsymbol{r})\right). \quad [24]$$

Note that this expression provides an estimate for the indirect free energy change only, because $\mathcal{V}_{R,AB}$ and $\mathcal{V}_{AB}$ do not include direct solute–solute pair interaction energies.

To determine the analog of Eq. **24** for the SS system, we note that the SS and FM systems have the same Gaussian-truncated solvent–solvent Coulomb interactions. The free energy changes given by the lower set of green arrows in Fig. 1 can then be readily determined by turning on the LMF potential $\mathcal{V}_{R1,AB}$ in Eq. **21** with a linear coupling parameter λ. Using standard coupling parameter techniques, the exact expression for $\Delta\bar{\Omega}^{fm,ss}_{AB}(r)$ is

$$\Delta\bar{\Omega}^{fm,ss}_{AB}(r) = \int_0^1 d\lambda \int d\boldsymbol{r}'\, \rho^{q}_{\lambda,AB}(\boldsymbol{r}'|\mathbf{0},\boldsymbol{r}) \mathcal{V}_{R1,AB}(\boldsymbol{r}'|\mathbf{0},\boldsymbol{r}), \quad [25]$$

where $\rho^{q}_{\lambda,AB}(\boldsymbol{r}'\,|\,\mathbf{0},\boldsymbol{r})$ is the induced charge density in state λ with potential $\lambda\mathcal{V}_{R1,AB}(\boldsymbol{r}'\,|\,\mathbf{0},\boldsymbol{r})$.

As discussed in SI appendix of Remsing et al. (30) leading to equation S16, because of the slowly varying nature of $\mathcal{V}_{R1,AB}$, the induced density should obey Gaussian statistics to a good approximation, which means that $\rho^{q}_{\lambda,AB}(\boldsymbol{r}'\,|\,\mathbf{0},\boldsymbol{r})$ in Eq. **25** can be accurately approximated by linear interpolation between its values at $\lambda = 0$ and $\lambda = 1$ (85). Thus Eq. **25** can be reduced to

$$\Delta\bar{\Omega}^{fm,ss}_{AB}(r) \approx \frac{1}{2}\int d\boldsymbol{r}' \left(\rho^{q}_{AB}(\boldsymbol{r}'|\mathbf{0},\boldsymbol{r}) + \rho^{q}_{0,AB}(\boldsymbol{r}'|\mathbf{0},\boldsymbol{r})\right)\mathcal{V}_{R1,AB}(\boldsymbol{r}'|\mathbf{0},\boldsymbol{r}). \quad [26]$$

Inserting results from Eqs. **24** and **26** into Eq. **16**, the approximate expression for $w^{ss}_{AB}(r)$ is then given by

$$\begin{aligned} w^{ss}_{AB}(r) \approx\ & w^{f}_{AB}(r) \\ & + \frac{1}{2}\int d\boldsymbol{r}'\, \rho^{q}_{AB}(\boldsymbol{r}'|\mathbf{0},\boldsymbol{r})\mathcal{V}_{1,AB}(\boldsymbol{r}'|\mathbf{0},\boldsymbol{r}) \\ & + \frac{1}{2}\int d\boldsymbol{r}'\, \rho^{q}_{0,AB}(\boldsymbol{r}'|\mathbf{0},\boldsymbol{r})\mathcal{V}_{R1,AB}(\boldsymbol{r}'|\mathbf{0},\boldsymbol{r}) \\ & - \frac{1}{2}\int d\boldsymbol{r}'\, \rho^{q}_{A}(\boldsymbol{r}'_A)\mathcal{V}_{1,A}(\boldsymbol{r}'_A) \\ & - \frac{1}{2}\int d\boldsymbol{r}'\, \rho^{q}_{0,A}(\boldsymbol{r}'_A)\mathcal{V}_{R1,A}(\boldsymbol{r}'_A) \\ & - \frac{1}{2}\int d\boldsymbol{r}'\, \rho^{q}_{B}(\boldsymbol{r}'_B)\mathcal{V}_{1,B}(\boldsymbol{r}'_B) \\ & - \frac{1}{2}\int d\boldsymbol{r}'\, \rho^{q}_{0,B}(\boldsymbol{r}'_B)\mathcal{V}_{R1,B}(\boldsymbol{r}'_B). \end{aligned} \quad [27]$$

However, even after the LMF and Gaussian approximations have been made, some terms in Eq. **27** still require averages over three-body correlation functions. In general, accurate point-wise approximations for such three-body functions are usually hard to get either analytically or numerically. But previous work (72) has shown that integrals over such functions when multiplied by slowly varying long-ranged interaction terms like $\mathcal{V}_{1,AB}$ and $\mathcal{V}_{R1,AB}$ can often be accurately approximated by assuming the charge density perturbations from each solute add independently. Thus we can use the approximation

$$\rho^{q}_{AB}(\boldsymbol{r}'|\mathbf{0},\boldsymbol{r}) \approx \rho^{q}_{A}(\boldsymbol{r}'_A) + \rho^{q}_{B}(\boldsymbol{r}'_B), \quad [28]$$

in expressions for the averages in Eq. **27**. As shown below, this uncorrelated density response preserves the asymptotic behavior of the solute–solute PMF, as would be expected, and in ref. 72 it gave surprisingly accurate results at much smaller r, provided that the solute cores do not overlap.

After making this additional approximation, many terms in Eq. **27** cancel. The final simple result, involving only solute–solvent correlation functions for isolated solutes, is given in Eq. **17**.

Asymptotic Behavior of the Effective Ion–Ion Interaction of the Short Solvent Model. To understand the asymptotic behavior of the effective ion–ion interaction $w^{ss}_{AB}(r)$, it is useful to take a Fourier transform of Eq. **17**, which gives

$$\begin{aligned} w^{ss}_{AB}(k) =\ & Q_A Q_B \hat{v}(k) \\ & + \frac{1}{2}\left(\hat{\rho}^{q}_{A}(k) + \hat{\rho}^{q}_{0,A}(k)\right) Q_B \hat{v}_1(k) \\ & + \frac{1}{2}\left(\hat{\rho}^{q}_{B}(k) + \hat{\rho}^{q}_{0,B}(k)\right) Q_A \hat{v}_1(k) \\ & + \frac{1}{2}\left(\hat{\rho}^{q}_{A}(k)\hat{\rho}^{q}_{0,B}(k) + \hat{\rho}^{q}_{B}(k)\hat{\rho}^{q}_{0,A}(k)\right)\hat{v}_1(k). \end{aligned} \quad [29]$$

Here $\hat{v}(k)$ is the Fourier transform of $v(r) = 1/r$,

$$\hat{v}(k) = \frac{4\pi}{k^2}, \quad [30]$$

and $\hat{v}_1(k)$ is the Fourier transform of $v_1(r) = \mathrm{erf}(r/\sigma)/r$,

$$\hat{v}_1(k) = \frac{4\pi}{k^2} e^{-k^2\sigma^2/4} = \frac{4\pi}{k^2} + \mathcal{O}(1). \quad [31]$$

$\hat{\rho}^{q}_{A}(k)$ is the Fourier transform of $\rho^{q}_{A}(r)$. Its expansion around $k = 0$ is

$$\hat{\rho}^{q}_{A}(k) = -\left(1 - \frac{1}{\epsilon}\right) Q_A + \mathcal{O}(k^2), \quad [32]$$

where ϵ is the dielectric constant of the full water solvent, and $(1-1/\epsilon)Q_A$ is the total water charge induced to screen the ion charge Q_A. Similar results hold for $\hat{\rho}^q_B(k)$.

In the short solvent model (and the Gaussian-truncated model) the electrostatic interaction between ions and water is truncated on a microscopic length scale. Thus the effective total charge of the ion and the associated screening charge of the solvent are also 0, which means that the expansion of $\hat{\rho}^q_{0,A}(k)$ and $\hat{\rho}^q_{0,B}(k)$ has no zeroth-order term:

$$\hat{\rho}^q_{0,A}(k) = 0 + \mathcal{O}(k^2). \quad [33]$$

Substituting Eqs. **30–33** into Eq. **29** gives

$$w^{ss}_{AB}(k) = \frac{1}{\epsilon} Q_A Q_B \frac{4\pi}{k^2} + \mathcal{O}(1), \quad [34]$$

and taking the inverse transform of Eq. **34** to go back to r space gives the asymptotic behavior of $w^{ss}_{AB}(r)$:

$$w^{ss}_{AB}(r) \sim \frac{1}{\epsilon} Q_A Q_B \frac{1}{r} \quad \text{when } r \to \infty. \quad [35]$$

This result is consistent with dielectric continuum theory.

1. C. Tanford, The hydrophobic effect and the organization of living matter. *Science* **200**, 1012–1018 (1978).
2. M. Belhadj, H. E. Alper, R. M. Levy, Molecular dynamics simulations of water with Ewald summation for the long range electrostatic interactions. *Chem. Phys. Lett.* **179**, 13–20 (1991).
3. U. Essmann *et al.*, A smooth particle mesh Ewald method. *J. Chem. Phys.* **103**, 8577–8593 (1995).
4. S. S. Yi, C. Pan, Z. H. Hu, Accurate treatments of electrostatics for computer simulations of biological systems: A brief survey of developments and existing problems. *Chin. Phys. B* **24**, 120201 (2015).
5. B. Roux, T. Simonson, Implicit solvent models. *Biophys. Chem.* **78**, 1–20 (1999).
6. W. C. Still, A. Tempczyk, R. C. R. Hawley, T. Hendrickson, Semianalytical treatment of solvation for molecular mechanics and dynamics. *J. Am. Chem. Soc.* **112**, 6127–6129 (1990).
7. D. Qiu, P. S. Shenkin, F. P. Hollinger, W. C. Still, The GB/SA continuum model for solvation. A fast analytical method for the calculation of approximate Born radii. *J. Phys. Chem. A* **101**, 3005–3014 (1997).
8. M. Schaefer, M. Karplus, A comprehensive analytical treatment of continuum electrostatics. *J. Phys. Chem.* **100**, 1578–1599 (1996).
9. T. Lazaridis, M. Karplus, Effective energy function for proteins in solution. *Proteins Struct. Funct. Bioinform.* **35**, 133–152 (1999).
10. R. A. Pierotti, A scaled particle theory of aqueous and nonaqueous solutions. *Chem. Rev.* **76**, 717–726 (1976).
11. C. Tanford, Interfacial free energy and the hydrophobic effect. *Proc. Natl. Acad. Sci. U.S.A.* **76**, 4175–4176 (1979).
12. N. A. Baker, Improving implicit solvent simulations: A Poisson-centric view. *Curr. Opin. Struct. Biol.* **15**, 137–143 (2005).
13. N. A. Baker, "Poisson-Boltzmann methods for biomolecular electrostatics" in *Methods in Enzymology*, A. M. Pyle, D. W. Christianson, Eds. (Academic Press, 2004), vol. 383, pp. 94–118.
14. D. Sitkoff, K. A. Sharp, B. Honig, Accurate calculation of hydration free energies using macroscopic solvent models. *J. Phys. Chem.* **98**, 1978–1988 (1994).
15. J. Wagoner, N. A. Baker, Solvation forces on biomolecular structures: A comparison of explicit solvent and Poisson-Boltzmann models. *J. Comput. Chem.* **25**, 1623–1629 (2004).
16. M. Nina, W. Im, B. Roux, Optimized atomic radii for protein continuum electrostatics solvation forces. *Biophys. Chem.* **78**, 89–96 (1999).
17. J. Chen, C. L. Brooks, J. Khandogin, Recent advances in implicit solvent-based methods for biomolecular simulations. *Curr. Opin. Struct. Biol.* **18**, 140–148 (2008).
18. W. Im, B. Roux, Ion permeation and selectivity of OmpF porin: A theoretical study based on molecular dynamics, Brownian dynamics, and continuum electrodiffusion theory. *J. Mol. Biol.* **322**, 851–869 (2002).
19. H. Gouda, I. D. Kuntz, D. A. Case, P. A. Kollman, Free energy calculations for theophylline binding to an RNA aptamer: Comparison of MM-PBSA and thermodynamic integration methods. *Biopolymers* **68**, 16–34 (2003).
20. R. Zhou, Free energy landscape of protein folding in water: Explicit vs. implicit solvent. *Proteins Struct. Funct. Bioinform.* **53**, 148–161 (2003).
21. J. Chen, C. L. Brooks, Critical importance of length-scale dependence in implicit modeling of hydrophobic interactions. *J. Am. Chem. Soc.* **129**, 2444–2445 (2007).
22. A. Masunov, T. Lazaridis, Potentials of mean force between ionizable amino acid side chains in water. *J. Am. Chem. Soc.* **125**, 1722–1730 (2003).
23. R. Zhou, G. Krilov, B. J. Berne, Comment on "can a continuum solvent model reproduce the free energy landscape of a β-hairpin folding in water?" The Poisson-Boltzmann equation. *J. Phys. Chem. B* **108**, 7528–7530 (2004).
24. O. Beckstein, K. Tai, M. S. P. Sansom, Not ions alone: Barriers to ion permeation in nanopores and channels. *J. Am. Chem. Soc.* **126**, 14694–14695 (2004).
25. J. H. Lin, N. A. Baker, J. A. McCammon, Bridging implicit and explicit solvent approaches for membrane electrostatics. *Biophys. J.* **83**, 1374–1379 (2002).
26. C. G. Ricci, B. Li, L. T. Cheng, J. Dzubiella, J. A. McCammon, Tailoring the variational implicit solvent method for new challenges: Biomolecular recognition and assembly. *Front. Mol. Biosci.* **5**, 1–10 (2018).
27. S. Zhou *et al.*, Variational implicit-solvent predictions of the dry–wet transition pathways for ligand–receptor binding and unbinding kinetics. *Proc. Natl. Acad. Sci. U.S.A.* **116**, 14989–14994 (2019).
28. Z. Chen, N. A. Baker, G. W. Wei, Differential geometry based solvation model I: Eulerian formulation. *J. Comput. Phys.* **229**, 8231–8258 (2010).
29. S. Zhou, L. T. Cheng, J. Dzubiella, B. Li, J. A. McCammon, Variational implicit solvation with Poission-Boltzmann theory. *J. Chem. Theory Comput.* **10**, 1454–1467 (2014).
30. R. C. Remsing, S. Liu, J. D. Weeks, Long-ranged contributions to solvation free energies from theory and short-ranged models. *Proc. Natl. Acad. Sci. U.S.A.* **113**, 2819–2826 (2016).
31. J. M. Rodgers, J. D. Weeks, Local molecular field theory for the treatment of electrostatics. *J. Phys. Condens. Matter* **20**, 494206 (2008).
32. B. Widom, Intermolecular forces and the nature of the liquid state. *Science* **157**, 375–382 (1967).
33. G. Hummer, L. R. Pratt, A. E. García, Free energy of ionic hydration. *J. Phys. Chem.* **100**, 1206–1215 (1996).
34. S. E. Feller, R. W. Pastor, A. Rojnuckarin, S. Bogusz, B. R. Brooks, Effect of electrostatic force truncation on interfacial and transport properties of water. *J. Phys. Chem.* **100**, 17011–17020 (1996).
35. C. J. Fennell, J. D. Gezelter, Is the Ewald summation still necessary? Pairwise alternatives to the accepted standard for long-range electrostatics. *J. Chem. Phys.* **124**, 234104 (2006).
36. L. Zhang, J. Han, H. Wang, R. Car, W. E, Deep potential molecular dynamics: A scalable model with the accuracy of quantum mechanics. *Phys. Rev. Lett.* **120**, 143001 (2018).
37. B. Cheng, E. A. Engel, J. Behler, C. Dellago, M. Ceriotti, Ab initio thermodynamics of liquid and solid water. *Proc. Natl. Acad. Sci. U.S.A.* **116**, 1110–1115 (2019).
38. A. Grisafi, M. Ceriotti, Incorporating long-range physics in atomic-scale machine learning. *J. Chem. Phys.* **151**, 204105 (2019).
39. J. A. McCammon, Darwinian biophysics: Electrostatics and evolution in the kinetics of molecular binding. *Proc. Natl. Acad. Sci. U.S.A.* **106**, 7683–7684 (2009).
40. P. L. Geissler, C. Dellago, D. Chandler, Kinetic pathways of ion pair dissociation in water. *J. Phys. Chem. B* **103**, 3706–3710 (2002).
41. A. J. Ballard, C. Dellago, Toward the mechanism of ionic dissociation in water. *J. Phys. Chem. B* **116**, 13490–13497 (2012).
42. M. Salanne, S. Tazi, R. Vuilleumier, B. Rotenberg, Ca^{2+}-Cl^- association in water revisited: The role of cation hydration. *ChemPhysChem* **18**, 2807–2811 (2017).
43. G. M. Torrie, J. P. Valleau, Nonphysical sampling distributions in Monte Carlo free-energy estimation: Umbrella sampling. *J. Comput. Phys.* **23**, 187–199 (1977).
44. Z. Tan, E. Gallichio, M. Lapelosa, R. M. Levy, Theory of binless multi-state free energy estimation with applications to protein-ligand binding. *J. Chem. Phys.* **136**, 144102 (2012).
45. M. R. Shirts, J. D. Chodera, Statistically optimal analysis of samples from multiple equilibrium states. *J. Chem. Phys.* **129**, 124105 (2008).
46. J. S. Hub, B. L. de Groot, D. van der Spoel, g_wham—A free weighted histogram analysis implementation including robust error and autocorrelation estimates. *J. Chem. Theory Comput.* **6**, 3713–3720 (2010).
47. M. Dal Peraro, S. Raugei, P. Carloni, M. L. Klein, Solute–solvent charge transfer in aqueous solution. *ChemPhysChem* **6**, 1715–1718 (2005).
48. Z. Zhao, D. M. Rogers, T. L. Beck, Polarization and charge transfer in the hydration of chloride ions. *J. Chem. Phys.* **132**, 014502 (2010).
49. T. Duignan *et al.*, Hydration structure of sodium and potassium ions with DFT-MD. ChemRxiv:7466426 (14 December 2018).
50. L. Zhou, J. Xu, L. Xu, X. Wu, Importance of van der Waals effects on the hydration of metal ions from the Hofmeister series. *J. Chem. Phys.* **150**, 124505 (2019).
51. F. Paesani, P. Bajaj, M. Riera, Chemical accuracy in modeling halide ion hydration from many-body representations. *Adv. Phys. X* **4**, 1631212 (2019).
52. S. Koneshan, J. C. Rasaiah, R. M. Lynden-Bell, S. H. Lee, Solvent structure, dynamics, and ion mobility in aqueous solutions at 25 °C. *J. Phys. Chem. B* **102**, 4193–4204 (1998).
53. M. Kohagen, P. E. Mason, P. Jungwirth, Accurate description of calcium solvation in concentrated aqueous solutions. *J. Phys. Chem. B* **118**, 7902–7909 (2014).
54. M. D. Baer, C. J. Mundy, Local aqueous solvation structure around Ca^{2+} during $Ca^{2+}\cdots Cl^-$ pair formation. *J. Phys. Chem. B* **120**, 1885–1893 (2016).
55. S. Mamatkulov, M. Fyta, R. R. Netz, Force fields for divalent cations based on single-ion and ion-pair properties. *J. Chem. Phys.* **138**, 024505 (2013).
56. N. F. A. Van Der Vegt *et al.*, Water-mediated ion pairing: Occurrence and relevance. *Chem. Rev.* **116**, 7626–7641 (2016).
57. S. Roy, M. D. Baer, C. J. Mundy, G. K. Schenter, Reaction rate theory in coordination number space: An application to ion solvation. *J. Phys. Chem. C* **120**, 7597–7605 (2016).
58. J. K. Denton *et al.*, Molecular-level origin of the carboxylate head group response to divalent metal ion complexation at the air–water interface. *Proc. Natl. Acad. Sci. U.S.A.* **116**, 14874–14880 (2019).
59. Y. Lee, D. Thirumalai, C. Hyeon, Ultrasensitivity of water exchange kinetics to the size of metal ion. *J. Am. Chem. Soc.* **139**, 12334–12337 (2017).

60. R. C. Remsing, M. L. Klein, Exponential scaling of water exchange rates with ion interaction strength from the perspective of dynamic facilitation theory. *J. Phys. Chem. A* **123**, 1077–1084 (2019).
61. M. D. Daily, M. D. Baer, C. J. Mundy, Divalent ion parameterization strongly affects conformation and interactions of an anionic biomimetic polymer. *J. Phys. Chem. B* **120**, 2198–2208 (2016).
62. E. Koculi, C. Hyeon, D. Thirumalai, S. A. Woodson, Charge density of divalent metal cations determines RNA stability. *J. Am. Chem. Soc.* **129**, 2676–2682 (2007).
63. N. Hori, N. A. Denesyuk, D. Thirumalai, Ion condensation onto ribozyme is site specific and fold dependent. *Biophys. J.* **116**, 2400–2410 (2019).
64. S. Moghaddam *et al.*, Metal ion dependence of cooperative collapse transitions in RNA. *J. Mol. Biol.* **393**, 753–764 (2009).
65. F. H. Stillinger, Structure in aqueous solutions of nonpolar solutes from the standpoint of scaled-particle theory. *J. Solut. Chem.* **2**, 141–158 (1973).
66. K. Lum, D. Chandler, J. D. Weeks, Hydrophobicity at small and large length scales. *J. Phys. Chem. B* **103**, 4570–4577 (1999).
67. D. Chandler, Interfaces and the driving force of hydrophobic assembly. *Nature* **437**, 640–647 (2005).
68. B. Widom, P. Bhimalapuram, K. Koga, The hydrophobic effect. *Phys. Chem. Chem. Phys.* **5**, 3085–3093 (2003).
69. L. A. Girifalco, Molecular properties of fullerene in the gas and solid phases. *J. Phys. Chem.* **96**, 858–861 (1992).
70. N. Choudhury, A molecular dynamics simulation study of buckyballs in water: Atomistic versus coarse-grained models of c60. *J. Chem. Phys.* **125**, 034502 (2006).
71. R. C. Remsing, J. D. Weeks, Dissecting hydrophobic hydration and association. *J. Phys. Chem. B* **117**, 15479–15491 (2013).
72. A. Gao *et al.*, Role of solute attractive forces in the atomic-scale theory of hydrophobic effects. *J. Phys. Chem. B* **122**, 6272–6276 (2018).
73. M. I. Chaudhari, S. A. Holleran, H. S. Ashbaugh, L. R. Pratt, Molecular-scale hydrophobic interactions between hard-sphere reference solutes are attractive and endothermic. *Proc. Natl. Acad. Sci. U.S.A.* **110**, 20557–20562 (2013).
74. M. I. Chaudhari, S. B. Rempe, D. Asthagiri, L. Tan, L. R. Pratt, Molecular theory and the effects of solute attractive forces on hydrophobic interactions. *J. Phys. Chem. B* **120**, 1864–1870 (2016).
75. T. Morawietz, A. Singraber, C. Dellago, J. Behler, How van der Waals interactions determine the unique properties of water. *Proc. Natl. Acad. Sci. U.S.A.* **113**, 8368–8373 (2016).
76. J. M. Rodgers, J. D. Weeks, Interplay of local hydrogen-bonding and long-ranged dipolar forces in simulations of confined water. *Proc. Natl. Acad. Sci. U.S.A.* **105**, 19136–19141 (2008).
77. R. C. Remsing, J. M. Rodgers, J. D. Weeks, Deconstructing classical water models at interfaces and in bulk. *J. Stat. Phys.* **145**, 313–334 (2011).
78. Z. Hu, Symmetry-preserving mean field theory for electrostatics at interfaces. *Chem. Commun.* **50**, 14397–14400 (2014).
79. C. Pan, S. Yi, Z. Hu, The effect of electrostatic boundaries in molecular simulations: Symmetry matters. *Phys. Chem. Chem. Phys.* **19**, 4861–4876 (2017).
80. C. Pan, S. Yi, Z. Hu, Analytic theory of finite-size effects in supercell modeling of charged interfaces. *Phys. Chem. Chem. Phys.* **21**, 14858–14864 (2019).
81. S. Yi, C. Pan, L. Hu, Z. Hu, On the connections and differences among three mean-field approximations: A stringent test. *Phys. Chem. Chem. Phys.* **19**, 18514–18518 (2017).
82. R. C. Remsing, J. D. Weeks, Alchemical free energy calculations and umbrella sampling with local molecular field theory. *J. Theor. Comput. Chem.* **17**, 1840003 (2018).
83. Y. Ishii *et al.*, Spatially-decomposed free energy of solvation based on the endpoint density-functional method. *J. Chem. Theory Comput.* **15**, 2896–2912 (2019).
84. R. C. Remsing, J. D. Weeks, Hydrophobicity scaling of aqueous interfaces by an electrostatic mapping. *J. Phys. Chem. B* **119**, 9268–9277 (2015).
85. C. Chipot, A. Pohorille, Eds., *Free Energy Calculations: Theory and Applications in Chemistry and Biology*, Springer Series in Chemical Physics (Springer, 2007), vol. 86.